Particle & Particle Systems Characterization
www.particle-journal.com

Deposition of Gold Nanoparticles on a Self-Supporting Carbon Foil

Philine Hepperle, Woon Yong Baek, Heidi Nettelbeck, and Hans Rabus*

Electron emission cross sections of gold nanoparticles (AuNPs) are important for assessing their radiosensitizing effects from ionizing radiation using Monte Carlo simulations. Measurements of these data require samples of sufficiently large area density, homogeneous nanoparticle distribution, and a mechanically stable sample holder to ensure a low background signal. While several methods exist for the deposition of nanoparticles, there is little information regarding the deposition of AuNPs in an aqueous solution onto a self-supporting film. The aim of this is to find suitable preparation techniques for AuNP samples which fulfill the above requirements. AuNP samples are produced using different deposition techniques and a 50 nm-thick carbon foil as the substrate. These samples are characterized with respect to the size and spatial distribution of AuNPs using a scanning electron microscope. The drop-casting technique yields the best results, while those obtained with the spin-coater technique are less reproducible regarding sample stability. The microdrop method is deemed unsuitable due to its tendency to form AuNP clusters. Measurements conducted with a synchrotron radiation source, as well as with protons and electrons, confirm the suitability of these samples for studying electron emission spectra of AuNPs for different radiation types.

1. Introduction

Gold nanoparticles (AuNPs) are gaining interest as radiosensitizing materials due to their advantageous chemical and physical properties. Nowadays, the techniques of AuNP synthesis are well developed. Size, shape, and surface of AuNPs can be controlled during synthesis, for example. by the methods of Frens, Enustun, and Turkevich.[1,2] Afterward, the AuNP surface can be functionalized in many different ways for drug delivery, as imaging agents or to bind to specific cells.[3,4] Wet-chemical synthesis of AuNPs is the most common preparation technique.

In recent years, the interest and use of AuNPs in medicine has significantly increased due to their excellent biocompatibility.[3,5,6] A broad range of possible applications in cancer diagnostics and treatment have been reported with special focus on their use in radiotherapy.[7–9] Radiotherapy is one of the standard methods for cancer treatment and is based on the damaging effect of ionizing radiation to cells.[8] Various studies have shown that the presence of AuNPs in cells during irradiation with X-rays or ions can lead to a considerable increase of cell killing, due to radiosensitizing effects of the AuNPs.[8–11] A localized presence of AuNPs in the tumor region may amplify tumor cell killing while reducing radiation damage to surrounding healthy tissue.[8]

One hypothesis for the enhanced cell killing is a local enhancement of the radiation dose within the target volume due to an increased emission of low-energy secondary electrons from the AuNPs.[10–16] The local dose enhancement near the AuNPs is generally assessed by Monte Carlo (MC) simulation, which is currently the most accurate method for radiation transport calculations.[12,17,18] While significant advances have been made with respect to the MC algorithms used to model radiation effects, particle transport simulations are still based on crude approximations. For example, most MC codes use physical models based on the first-order Born approximation to calculate electron emission cross sections. This approximation is, however, only valid for electron energies greater than a few keV. Considering that secondary electrons with energies below a few keV are responsible for most of the radiation damage, there is a need to improve MC physical models by providing experimental electron emission cross section data at these low energies. Previous experiments on X-ray-induced low-energy electron emission from AuNPs have revealed large discrepancies with results obtained by MC simulation.[19] Hence, the motivation to acquire more reliable electron emission data from AuNPs, especially for the Auger cascades following inner-shell ionizations that lead to the production of a high number of low-energy secondary electrons.[11–13]

P. Hepperle, W. Y. Baek, H. Nettelbeck
Physikalisch-Technische Bundesanstalt (PTB)
Bundesallee 100, 38116 Braunschweig, Germany
E-mail: philine.hepperle@ptb.de
P. Hepperle
Institute of Radioecology and Radiation Protection
Leibniz University Hannover
Herrenhäuserstraße 2, 30419 Hannover, Germany
H. Rabus
Physikalisch-Technische Bundesanstalt (PTB)
Abbestraße 2–12, 10587 Berlin, Germany
The ORCID identification number(s) for the author(s) of this article can be found under https://doi.org/10.1002/ppsc.202200136.

DOI: 10.1002/ppsc.202200136

For the precise measurement of electron emission spectra of AuNPs irradiated with X-ray, proton, and electron beams as a function of the AuNP parameters (i.e., size, shape, and distribution), the AuNP samples must fulfill several requirements.

First, the number of background electrons released from the substrate on which AuNPs are deposited should be as low as possible. Second, the sample must be stable enough to withstand the mechanical stress during the pumping procedure as an electron energy analyzer is operated in a high vacuum. Third, the sample substrate should be as thin as possible for the measurements with charged particles such as ions or electrons. This property is also important for a characterization of the AuNP distribution on the substrate using scanning electron microscopy (SEM) and scanning transmission electron microscopy (STEM). For this reason, a thin self-supporting film of a low-Z material is preferable. In this work, a carbon foil with a thickness of 50 nm was used as the substrate as it provided sufficient mechanical stability to be self-supported over the 5 mm aperture of the target holder.

The use of a thin self-supporting carbon foil imposes challenges in depositing the AuNPs uniformly over the substrate with a high reproducibility. Although different methods for the deposition of nanoparticles can be found in the literature, there is no mention regarding the deposition of AuNPs in an aqueous solution onto a thin self-supporting film.

This present work investigates the different deposition techniques reported in the literature for bulk substrates to determine whether they are suitable for use with a thin 50 nm-thick self-supporting carbon foil. To establish the most appropriate technique, AuNP samples were prepared using different methods and then analyzed with respect to the area density and homogeneity of the AuNP distribution. The spatial distribution of AuNPs on the carbon foil was characterized by means of SEM.

2. Results and Discussion

2.1. Sample Preparation Techniques

Several techniques for the deposition of AuNPs have been reported in the literature.[20–40] Selecting the best-suited deposition technique depends on the size, shape, and surface coverage of the medium in which the nanoparticles are present as well as the carrier material. One of the major difficulties is to achieve a macroscopically large homogeneous deposition area of nanoparticles with minimal clustering.[20,21]

The AuNPs used in this work were prepared wet-chemically. They were present in an aqueous solution and deposited on a self-supporting carbon foil of 50 nm thickness.

2.1.1. Vapor Deposition Techniques

Uniform AuNP distribution can be obtained by means of chemical and physical vapor deposition techniques, such as vacuum evaporation, thermal vaporization, electron beam evaporation, or sputtering.[23] In evaporation processes, the sample to be deposited is initially in a solid state. The sublimation of the sample from the solid phase to a vapor phase, which is applied to a substrate, leads to the formation of a thin film. In sputtering, the sample atoms are transferred from the target to the substrate by bombarding the target with energetic ions.[24,25] Since the AuNPs used in this study are present in an aqueous solution, these techniques are unsuitable.

2.1.2. Langmuir–Blodgett and Wet-Chemical Techniques

The widely used Langmuir–Blodgett (LB) technique, which is known to produce highly ordered, well-defined, ultra-thin mono- and multilayers, would be a suitable method for AuNPs in solution. In the first step, a floating monolayer, the so-called Langmuir film, is produced at the air–water interface. In the second step, this monolayer formed on the surface of the aqueous solution is deposited on a solid substrate by immersing the substrate into the solution and shearing off the film, similar to the dip-coating method.[21,26–30] Tests performed in this work, however, revealed that this deposition technique was unsuitable for the deposition of AuNPs on a thin carbon foil attached to a metallic sample holder. When immersed in an aqueous solution, the carbon foil was found to detach from the sample holder and float to the surface. This problem also excludes the use of wet-chemical deposition techniques such as electrochemical, galvanic, electrophoretic, or chemical bath deposition that are based on a chemical reaction in which reactants combine to form a product and thereby coat a surface.[23,31,32] As these take place in a solution, they are unsuitable for the same reason as the LB-technique described above.

2.1.3. Drop-Casting

Drop-casting is a simple method to deposit AuNPs on small substrates (≈1 cm^2).[20] In this method, the AuNP solution is dropped onto a substrate, where the solution spreads out and the liquid droplet evaporates. The meniscus of the droplet is pinned to the contact line.[21] Since the thin water layer at the boundary of the drop evaporates more quickly than in the droplet center, which leads to a capillary flow of the AuNP solution from the center to the boundary, a so-called coffee-ring consisting of multilayers usually forms. In addition, numerous islands of AuNPs form in the middle of the droplet.[21,26,33] A disadvantage of this method is that despite controlled conditions, evaporation rates may vary across the substrate. Variations in the concentration of the solution also lead to different film thicknesses and internal structures. Furthermore, the drop-casting technique has the disadvantage that large areas of monolayers with high reproducibility are not possible.[21,33]

2.1.4. Microdrop

The microdrop technique is based on the same principle as drop-casting. However, it allows a well-defined number of drops with volumes in the picoliter range to be deposited at a specific position. As small droplets evaporate quickly, the spatial distribution of AuNPs can be well controlled by subsequently

dispensing the drops at the required positions. It is even possible to deposit several drops at one position. Macis et al. showed in their work that a more homogeneous deposition can be achieved by using the microdrop technique.[34]

2.1.5. Spin-Coating

Spin-coating is an effective method for distributing particles on a substrate.[35,36] Compared to drop-casting, spin-coating allows larger areas of uniform deposition over the entire substrate (at room temperature) in a significantly shorter time.[36–38] In this technique, a drop of the nanoparticle solution is placed in the center of the substrate, which is then centrifuged. Centrifugal forces lead to an even distribution of the drop over the substrate followed by evaporation of the remaining volatile solvent.[36,39] The area and thickness of the particle layer depends on the concentration of the nanoparticles in the solution, the volume of the droplet, and the rotational speed.[35,36]

In this work, the drop-casting, spin-coating, and microdrop technique were used to prepare AuNP samples on a 50 nm-thick carbon foil. The produced samples were then investigated with respect to the requirements specified above.

2.2. Samples Prepared by the Microdrop Technique

The microdrop technique involves applying several drops of the AuNP solution at selected positions so that the nanoparticles can agglomerate drop by drop and build up a large monolayer. However, first attempts showed that the concentration of the AuNP solution was too high and led to clogging of the tip of the microdrop pipette. In order to avoid this clogging, the AuNP solution had to be diluted. SEM measurement of the samples prepared using the microdrop technique with a diluted AuNP solution, which can be seen in Figures S1 and S2, Supporting Information, reveal the formation of AuNP clusters and net-like structures. Diluting the solution did not yield thinner layers, but rather smaller clusters. When the AuNP concentration was further diluted to avoid clusters while keeping the volume of the drops constant and ensuring that the drops can be positioned exactly, almost no nanoparticles were detected in SEM measurements. Hence, the microdrop technique was deemed unsuitable for the production of large areas of high-density monolayers of AuNPs.

2.3. Samples Prepared by Drop-Casting

Figure 1a shows an SEM image of a dried AuNP drop following drop-casting in secondary electron (SE2) mode. Looking at the contour of the drop, it is evident that it is not perfectly circular. This may be attributed to sagging of the carbon foil due to the weight of the drop. Consequently, the drop congregates in the center of the foil and dries. At the boundary of the drop, the so-called coffee-ring effect occurs (refer to Figure 1b). As described above, this effect appears due to the fast evaporation of the volatile solvent of the droplet at its outer boundary. When the volatile solvent evaporates, a contact line forms at the air–water interface of the drop's perimeter since it is there that the thin liquid layer evaporates the fastest.[21,26,33] This leads to an additional capillary flow of the AuNP containing solvent to the perimeter, thus enhancing the area density of the AuNPs.[41] Consequently, clusters of AuNPs and multilayers form at the perimeter such that a saturated boundary area is created in which individual nanoparticles can no longer be distinguished. This leads to ring-like structures known as coffee-rings. In addition, it is also possible for sparse islands of AuNPs to form in the center of the droplet.[21,41,42]

At the center of the drop, another artifact can be seen which can be traced back to characteristic stress cracking of the carbon foil (refer to Figure 1a and **Figure 2**a). This stress cracking occurs when the drop starts to evaporate and the foil dries. During this process, the foil can contract and form wrinkles or cracks. The spontaneous formation of a universal self-similar wrinkle hierarchy under boundary confinement is a characteristic of any thin foil. Thin foils are unstable under boundary or substrate-induced pressure loads. Compression arising from the drying of the AuNP drop leads to a regular formation of wrinkles.[43,44] This results in the self-supporting area of the carbon foil on the target aperture no longer being smooth and homogeneous, thus making it difficult to obtain a macroscopically large deposition area of nanoparticles with as little clustering as possible.[20,21] From the enlarged STEM image in Figure 2b, almost no AuNPs can be seen in the middle of a crack, as expected. Starting from the boundary of the crack,

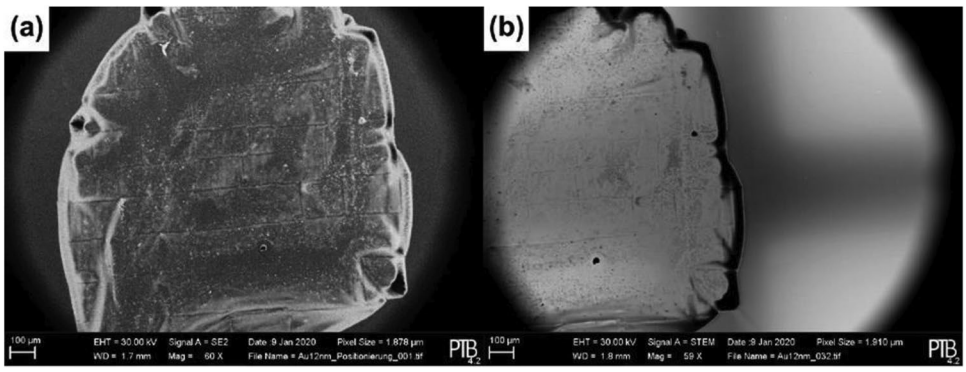

Figure 1. a) SE2 image of a sample prepared by casting a 0.5 µL droplet of 12 nmol L^{-1} AuNP solution containing 12 nm AuNPs onto a 50 nm carbon foil and b) STEM image of the boundary region of the evaporated drop with a visible coffee-ring.

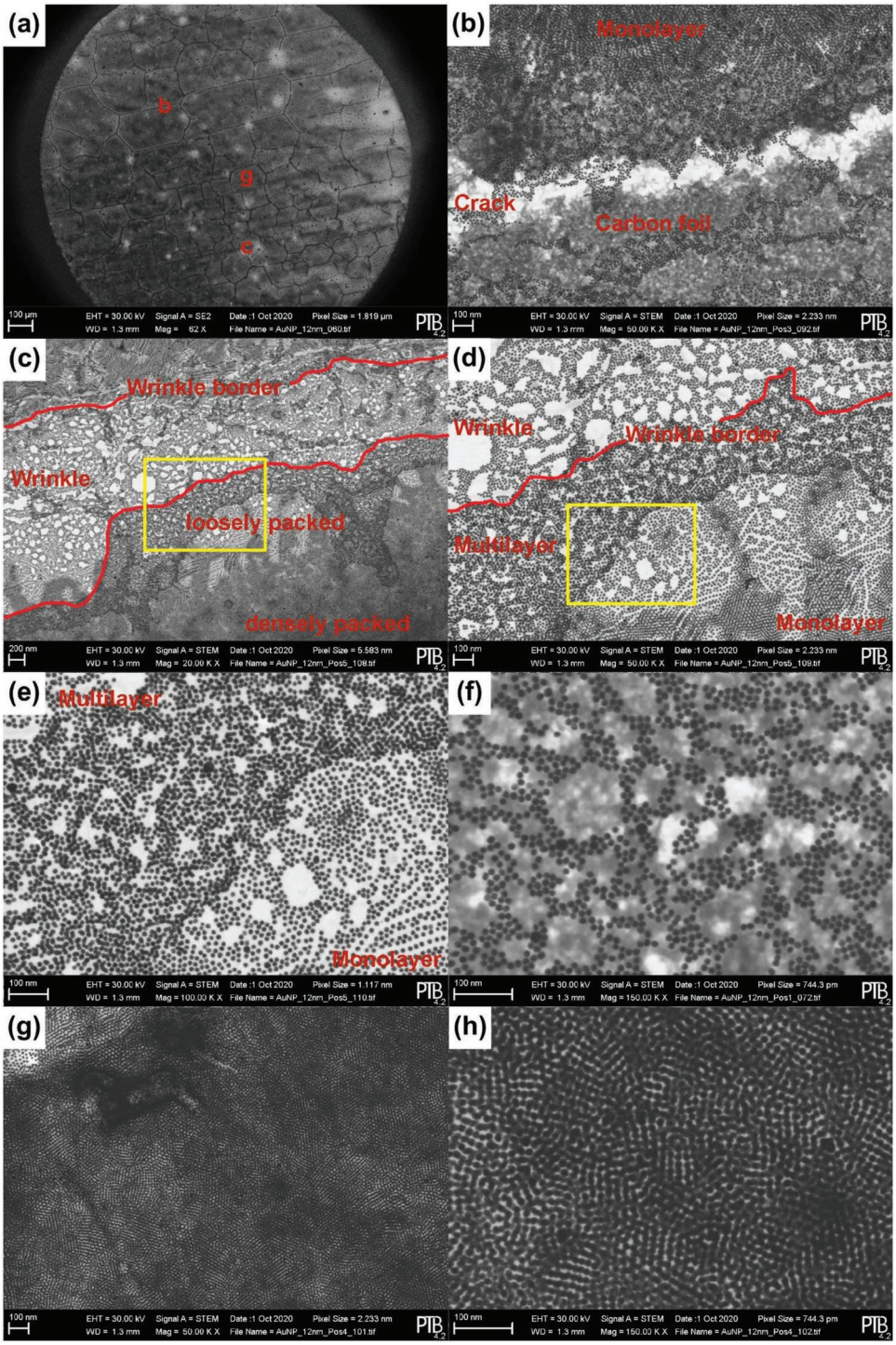

Figure 2. a) SE2 image of the characteristic stress cracking of the carbon foil in the middle of the drop. The locations are marked with the red letters b, c, and g. b) Enlarged STEM image of a crack. c–f) Distribution of AuNPs within the vicinity and on top of a wrinkle taken with increasing magnification (subsequent images are the magnifications of the yellow boxes in the prior image). On top of the wrinkle, AuNPs show net-like structures. Within the vicinity of a wrinkle, AuNPs form monolayers while clusters and multilayers are produced further away from the wrinkle. g) STEM image of a region between wrinkles and cracks, where AuNPs form large-scale monolayers. h) Magnified image of (g) showing a close-packed monolayer of AuNPs.

AuNPs seem to first form monolayers and then clusters, which merge into multilayers. The same behavior can be observed for wrinkles (Figure 2c,d). As opposed to cracks, however, the nanoparticles in wrinkles are present as monolayers and form net-like structures (Figure 2e,f). Kunstmann-Olsen et al. showed similar net-like distribution patterns and clustering of AuNPs after drop casting on carbon-coated transmission electron microscopy (TEM) sample grids.[45] On the wrinkles,

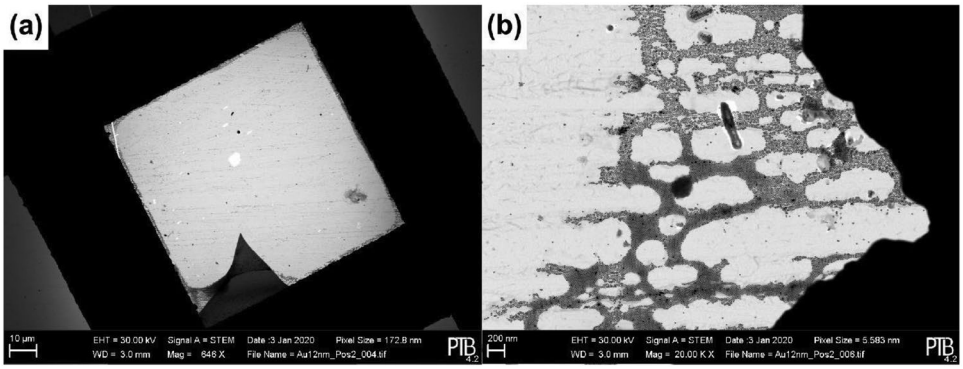

Figure 3. a) STEM image of a TEM copper grid mesh supporting the 50-nm-thick carbon foil. The AuNP droplet was deposited on the carbon foil using the drop-casting technique. The AuNPs can be seen to accumulate at the edges of the mesh, while no AuNPs appear in the center of a mesh. b) Magnified image of a corner of the copper grid which shows clustered AuNPs along the grid mesh.

the AuNPs start to cluster and form multilayers (Figure 2c–e), while between the wrinkles and cracks larger areas of monolayers are formed (Figure 2g,h). A monolayer as shown in Figure 2h would be the optimal structure for measurements of cross sections for electron emission from AuNPs as their mean number per area is well defined and can be determined with low uncertainty. In this structure, individual AuNPs can be resolved. However, disturbances such as wrinkles or cracks in the foil may lead to the formation of multilayers in which the nanoparticles can no longer be resolved from each other (compare the structure at the top of Figure 2g).

In order to eliminate sagging and increase surface smoothness of the carbon foil on the target holder, thereby reducing wrinkles, cracks, and thus clusters, a copper grid was used to support the carbon foil. **Figure 3**a shows the STEM image of a section of the carbon foil coated with drop-cast AuNPs, where the foil is supported by a single mesh of the copper grid underneath. A closer look at Figure 3b reveals clusters of AuNPs at locations where the carbon foil rests on the copper grid mesh. In contrast, no nanoparticles can be detected inside the grid mesh. The use of a copper grid to support the carbon foil is therefore not suitable for creating large areas of monolayers.

Deposition using the drop-casting technique provides sufficiently large AuNP layers. In this case, the surface coverage is defined as the occupancy of the carbon foil surface containing AuNPs for the examined section (e.g., the STEM image section). In the region of monolayers with net-like distribution pattern or islands, between 15% and 40% of the carbon surface is covered by AuNPs. In the area of large-scale monolayers (refer to Figure 2g,h) and multilayers, the mean relative surface coverage of nanoparticles on the carbon foil is between 60% and 80%. Further data regarding the surface coverage can be found in the Supporting Information.

Several samples were prepared by drop-casting using the same AuNP solution, carbon foil, and target holder. They were examined both with SEM and STEM. Depending on the degree of sagging of the self-supporting carbon foil, the drop was observed to spread and dry out differently each time. As described above, the wrinkles and resulting cracks form different deposition structures, which inhibit a reproducible deposition pattern. However, it is possible to make statements about the macroscopic proportions of surface areas covered with AuNPs monolayers, clusters, and multilayers. Thus, it is not the detailed microscopic deposition pattern, but rather the mean area density of AuNPs on the carbon foil in macroscopic dimensions (i.e., on the millimeter scale) that is reproducible.

2.4. Samples Prepared by Spin-Coating

Placing the sample holder covered with the carbon foil directly on the spin-coater led to rupture of the foil as it was sucked in by the vacuum of the spin-coater. Alternatively, the sample holder was fixed to a wafer using TEM glue which was then placed on the spin-coater. This method was also found to be unsuitable since the sample holder must be heated to remove the TEM glue when detaching it from the wafer. This application of heat led to cracking in the foil due to temperature stress. Fixing the sample holder onto a wafer with double-sided adhesive tape also resulted in cracking of the foil. Detaching the sample holder from the double-sided adhesive tape leads to the presence air beneath the foil, where the simultaneous pressure of air from above results in cracking of the carbon foil. The best method that allowed the removal of the holder after spin coating whilst minimizing foil cracking was the use of adhesive tape to fix the upper side of the sample holder to the wafer.

In our previous tests, spin-coating of a droplet of the AuNP solution was applied on a solid substrate coated with a 50 nm-thick carbon foil. The best results regarding distribution and drying of the droplet without any cracking of the foil were obtained with a rotational speed of 1000 rpm applied for a duration of 60 s. These parameters were also used in this work for the spin-coating of AuNPs on a self-supporting carbon foil. As described above, the spin-coating process consists of applying the AuNP solution on the carbon foil, accelerating and spinning of the sample by centrifugal forces, followed by evaporation of the remaining solvent. During the rotation of the sample, a spherical shaped droplet formed at the center of the sagging foil. This spherical droplet remained throughout the entire spin-coating process, eventually drying after several repetitions of the rotation program. The number of cycles, however, varied for each sample depending on the degree of foil sagging, and thus it was difficult to obtain reproducible deposition of AuNPs.

Samples produced using a spin-coater were analyzed with SEM and STEM, where any differences in the AuNP distribution from the two deposition techniques (drop-casting and spin-coating) were also investigated. When comparing the shape of the drop following spin coating in the SE2 images of **Figure 4**b, a more circular drop can be seen than that obtained using the

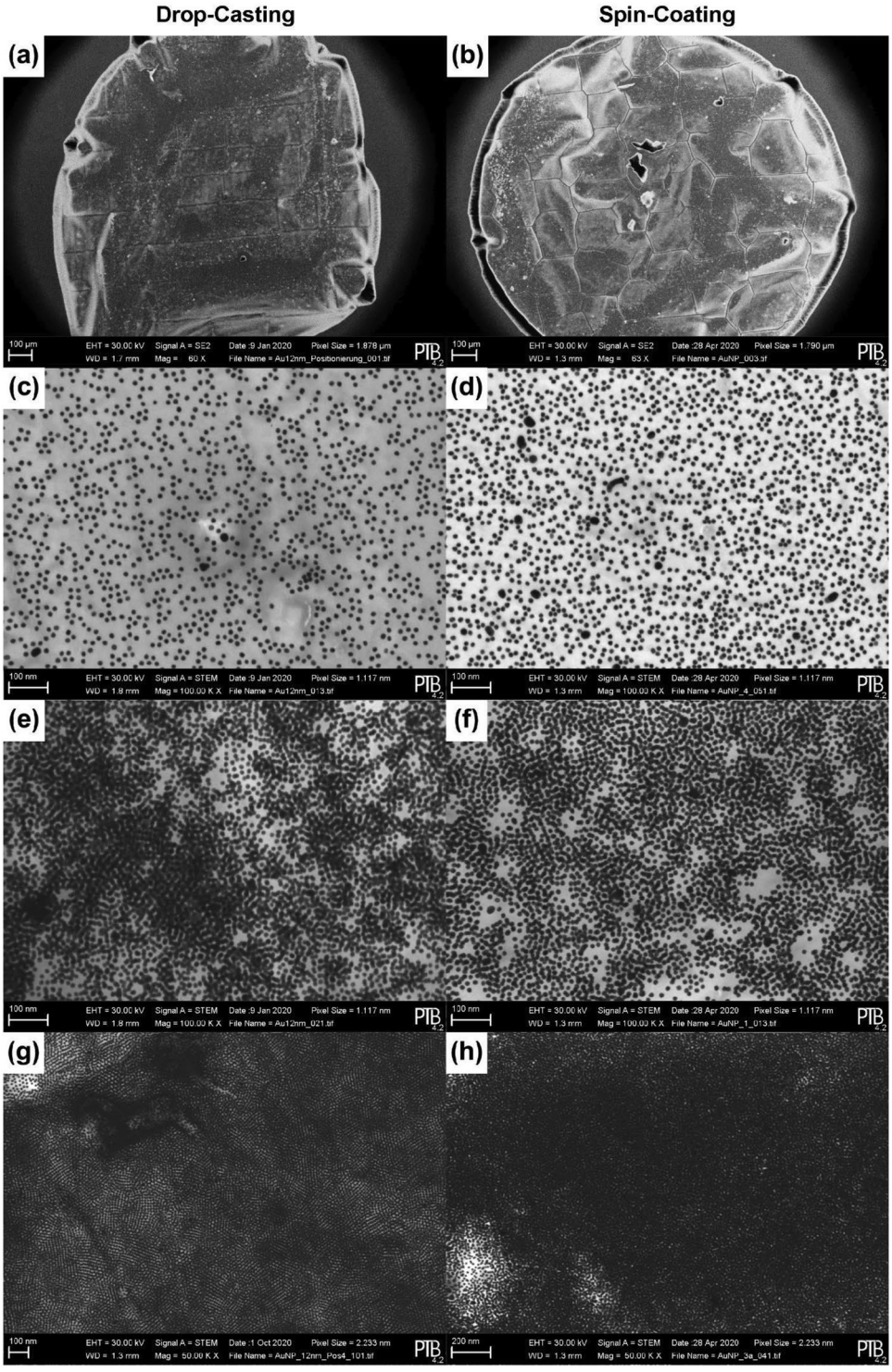

Figure 4. a) SE2 image of a 0.5 µL droplet of 12 nmol L^{-1} AuNP solution containing 12 nm diameter AuNPs deposited on a 50 nm-thick carbon foil using the drop-casting technique, b) SE2 image of a 0.5 µL droplet of 12 nm diameter AuNPs spin-coated on a 50 nm-thick carbon foil. STEM images of the distribution of the AuNPs on the carbon foil showing c) a monolayer after drop-casting, d) a monolayer after spin-coating, e) clusters and multilayers after drop-casting, f) clusters and multilayers after spin-coating, g) a surface area with large-scale mono- and multilayers after drop-casting, and h) multilayers after spin-coating.

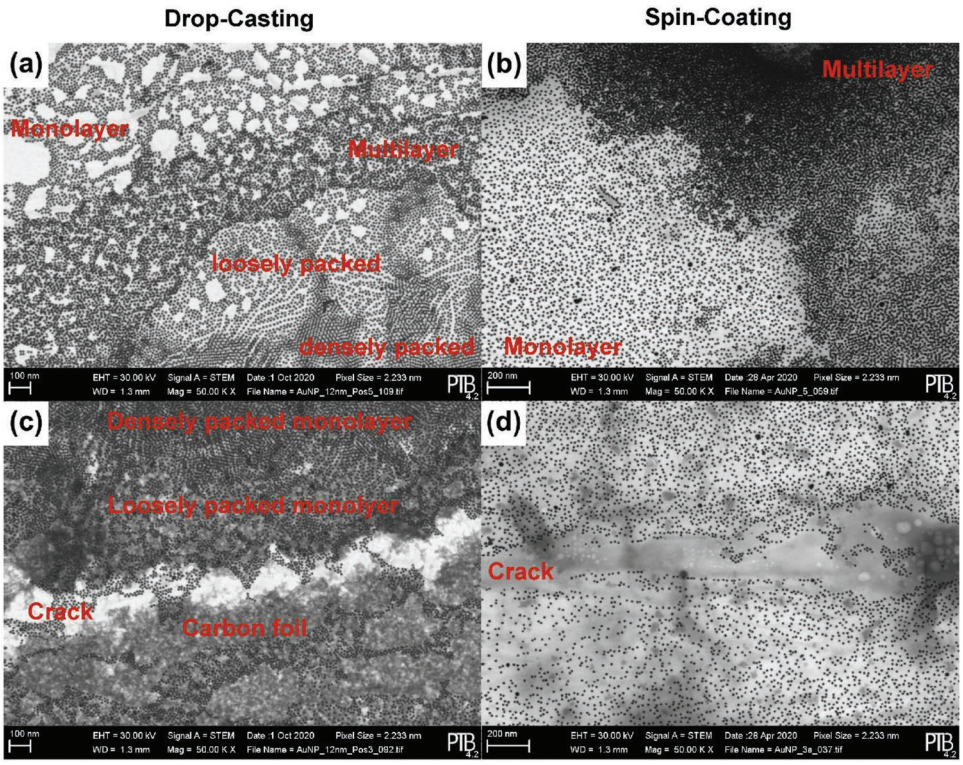

Figure 5. STEM image of the AuNP distribution in the transition region from a monolayer to a multilayer when using the a) drop-casting and b) spin-coating techniques. STEM image of the AuNP distribution within a crack or on a wrinkle when using the c) drop-casting and d) spin-coating techniques. Almost no AuNPs can be observed in the cracks.

drop-casting technique (Figure 4a). In the case of deposition by drop-casting technique, on the other hand, the so-called coffee-ring effect was also visible after spin-coating (refer to Figure 4b). A saturated boundary area, where individual AuNPs cannot be resolved, was also observed. Figure 4c–h exhibits no significant differences in the macroscopic pattern of AuNP distributions with both techniques. Figure 4d,f shows AuNPs in monolayers. AuNPs in clusters and multilayers are shown in Figure 4f,h. In the case of drop-casting, the mean surface coverage of AuNPs was between 15% and 40% for spin-coating and monolayers and between 60% and 80% in regions of multilayers. For the sample in Figure 4d, a surface coverage of 25% was determined, which is within the range of the mean surface coverage for drop-casting (between 15% and 40%). In comparison, the surface coverage of the sample produced by means of drop-casting technique in Figure 4c was 17%. In the area of multilayers, a surface coverage of 60% was achieved for the spin-coated sample shown in Figure 4f. In the case of the drop-casting technique, this surface coverage amounted to 71% (see Figure 4e). In the area of the densely packed multilayers, the surface coverage was also comparable: 96% for spin-coating (Figure 4h) and 87% for drop-casting (Figure 4g).

The distribution in the transition zone from a monolayer to a multilayer is also comparable for both techniques (**Figure 5**a,b). Similar distributions can be seen at the site of a wrinkle or a crack. Almost no AuNPs can be detected in the crack or wrinkle (Figure 5c,d).

Differences in the distribution of AuNPs when using the spin-coating instead of the drop-casting technique can be seen at the center of the samples. STEM images of the sample's center produced with the spin-coating technique (**Figure 6**a,b) reveal different packing densities compared to the samples obtained using the drop-casting technique. The nanoparticles, which were observed to form net-like structures, were often present as monolayers with a lower packing density. This is expected as in the case of spin-coating technique, the centrifugal force enhances the dispersion of the AuNPs in addition to the capillary flow.

In summary, the drying process of the AuNP drop has similarities to the drop-casting technique. However, the additional centrifugal dispersion force in the case of the spin-coating technique does not hinder the formation of clusters and multilayers. It is difficult to achieve a macroscopically large monolayer deposition of nanoparticles.

2.5. Electron Emission Measurements of Drop-Cast AuNPs on Self-Supporting Carbon Foils

Samples produced by drop-casting were characterized with respect to the spatial distribution of the AuNPs by irradiating them with X-rays and recording the number of electrons emitted. X-rays were generated by the synchrotron radiation source PETRA III on the P22 beamline at DESY in Hamburg, Germany. The AuNP distribution was measured by varying the

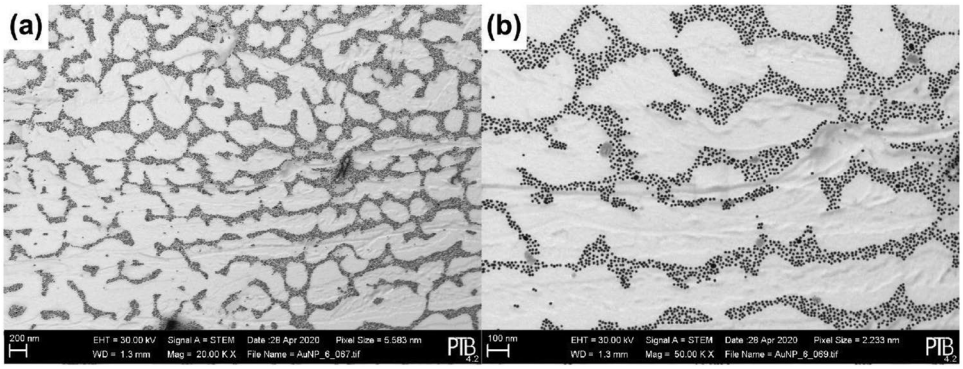

Figure 6. a) STEM image taken from the center of the droplet, showing a net-like distribution of 12 nm diameter AuNPs spin-coated on 50 nm-thick carbon foil and b) magnification of the same area of the image showing a net-like monolayer of AuNPs.

beam impinging point on the sample. **Figure 7** shows the variation of the signal of gold $L_3M_4M_5$ Auger electrons (at 7447 eV energy) when a 14.4 keV photon beam is scanned over a 3 mm distance along the diameter of the area covered with AuNPs (i.e., from about 1 mm before the droplet until ≈1 mm beyond it) in order to establish the droplet's boundary. The incidence angle of the photon beam to the sample was 15° and the beam was scanned perpendicular to the plane of incidence.

In the range between the scanning positions $d = 1.6$ mm and $d = 2.08$ mm, the photon beam strikes uncoated regions of the carbon foil (see Figure 7a). When the beam hits the outer boundary of the AuNP distribution, the electron count rate rapidly increases. The first maximum at $d = 2.21$ mm is attributed to scanning across the coffee-ring (see Figure 7b), which coincides with the saturated edge area of the drop. After passing this saturated edge, the count rate decreases toward the center of the sample where it fluctuates around a mean value until reaching the location of the coffee-ring on the perimeter of the droplet at $d = 3.55$ mm. Between these two peaks (coinciding with the coffee ring), the signal is constant with a relative standard deviation of 16% of the mean. This indicates that the AuNPs in the interior region of the sample comprise of monolayers, clusters, and multilayers. In this region, however, there are no dense clusters such as those observed in the saturated edge area. The average area density of gold atoms within the area of the photon beam (0.1 mm × 0.4 mm FWHM) has a relative uncertainty of 16%. Beyond the peak regions, the low electron intensity stems from the carbon foil having a photon absorption cross section that is significantly lower than that of gold, which leads to the emission of fewer electrons.

The separation between the two peaks is about 1.34 mm, which corresponds to the 1.41 mm diameter of the droplet estimated from Figure 7b. The width of both peaks at the signal level indicated by the green line in Figure 7a, which corresponds to about 40% of the peak height and the mean of the normalized signal at the sample's center, is about 0.10 mm. The mean width of the coffee-ring determined at 100 different positions using the software ImageJ (compare Figure 7b) amounts to 0.051 mm with a standard deviation $s = 0.019$ mm.[46,47] This large standard deviation is due to the fact that the coffee-ring rapidly varies with width, as can be seen in Figure 7b. For example, it was determined to be as low as 0.038 mm at one evaluated position and as high as 0.091 mm at another. The peak width can therefore vary depending on where the scan crosses the coffee-ring.

The signal shape in Figure 7a exhibits broadening due to the finite extension of the photon beam. The photon beam profile was therefore unfolded iteratively by means of the gradient search method from the measured signal profile. It was assumed that the photon beam profile along the scan direction can be

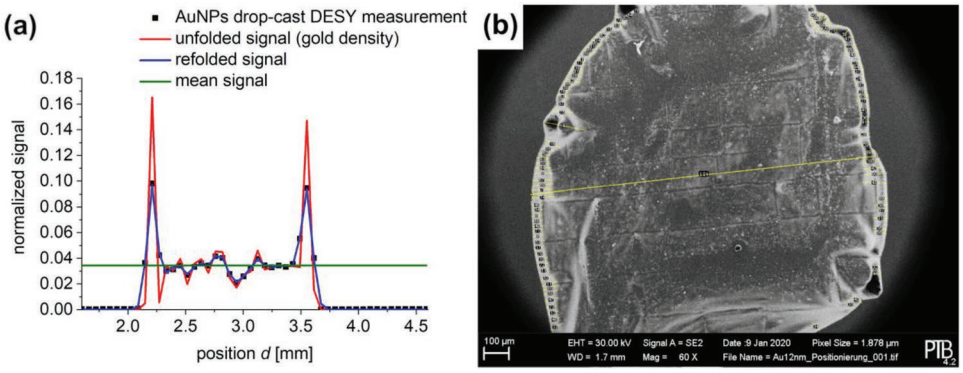

Figure 7. a) Dependence of the signal of 7447 eV electrons emitted along the scanned position of the photon beam on the sample, normalized to the area under the curve. The black symbols are the experimental data and blue curve represents the refolded profile. b) SE2 image of a sample prepared by casting a 0.5 µL droplet of solution containing 12 nm diameter AuNPs on a 50 nm-thick carbon foil, where the mean diameter of the droplet coincides with that of the coffee-ring.

represented by a Gaussian function with FWHM = 0.1 mm, which corresponds to the photon beam diameter. It was also assumed that the beam extension in the direction perpendicular to the scan direction (i.e., about 0.4 mm on the sample surface) does not have a significant influence. The result of this unfolding (red curve) was an estimate of the area density distribution of AuNPs. In the coffee-ring regions, this area density was about a factor of four higher than that in the plateau region. Refolding the estimated area density of AuNPs with the Gaussian beam profile resulted in the blue curve in Figure 7a, which coincides with the measured signal.

It can therefore be concluded that the width of the coffee-ring as determined from the distribution of AuNPs in the peaks is of a similar order of magnitude to that determined from the STEM images using the software ImageJ. Uncertainties in the peak widths arise from smearing of the peaks by smooth transition of the coffee-ring to multilayers as well as variations in the width of the coffee-ring (as evident in STEM measurements). The coffee-ring can thus be used as a "guide" for adjusting the position of the sample with respect to the beam. Measurements should therefore be conducted in the area between the peaks to avoid significant variations in the area density of AuNPs.

3. Conclusions

The deposition of AuNPs on a self-supporting carbon foil was carried out using different techniques, where deposition by drop-casting produced the best results. AuNPs were observed to form a sufficiently large area of monolayers suitable for measurement of electron emission spectra, however, the formation of clusters and multilayers could not be avoided. While the spatial distribution of AuNPs on a microscopic level is irreproducible, there does exist some macroscopic characteristics that are reproducible if the initial preparation conditions (i.e., AuNP solution, foil and temperature) remain the same.

In each sample, the AuNPs formed coffee-rings and monolayers as well as clusters that merged into multilayers. Monolayers of nanoparticles were found to be more easily produced when a solid and not self-supporting substrate was used. In the case of a thick solid substrate, however, measurements of electrons emitted in the forward direction following the impact of charged particles were not possible since the incident particles could not pass through the substrate. Similarly, the measurement of electron emission in the backward direction is also difficult due to the high background arising from electrons released from the substrate surface. The production and characterization of AuNP samples over the course of 1 year showed comparable distributions in terms of average area density of AuNPs over an area of about 6 mm^2. Despite the irreproducibility of the exact distribution on a microscopic scale, the consistency in the average area density for different samples allows one to study the dependence of electron emission cross section on AuNP parameters (i.e., size and coating material) upon ion or electron impact. The use of a copper grid mesh for the self-supporting carbon foil to eliminate foil sagging resulted in the tendency for AuNPs to cluster on the grid mesh, and hence, this approach was abandoned. Deposition by spin-coating on carbon foils provided similar results to those obtained using deposition by drop-casting. The microdrop technique, on the other hand, was found to be unsuitable for the deposition of AuNP solutions due to clogging of the pipette tip when dispensing the required concentrations to obtain a monolayer.

Initial measurements of electron emission spectra from AuNPs irradiated with X-rays, electrons, or protons have been carried out using the samples prepared in this work. These results indicate that the area density of AuNPs was sufficiently high to produce a good signal to background ratio. In addition, no damage or degradation of the samples was observed during their insertion into a vacuum environment nor during the measurements. In summary, this work shows that the deposition of AuNPs on thin self-supporting carbon foils using the drop-casting and spin-coating technique provides suitable AuNP targets for measurement of electron emission cross sections for photons and charged particles.

More detailed quantitative analysis of the AuNP distribution using small-angle X-ray scattering (SAXS), X-ray photoelectron spectroscopy (XPS), or attenuated total reflection (ATR) spectroscopy is envisaged as a continuation of this work. These results, together with electron emission spectra from AuNPs following irradiation with X-rays, electrons, and protons, will be reported in an additional paper.

4. Experimental Section

Materials: AuNPs in an aqueous solution (c = 12 nmol L^{-1}) with a mean diameter of 12 nm and a polyethylene glycol (PEG)-11-mercaptoundecanoic acid (MUA) coating were provided by the University Medical Center Hamburg-Eppendorf (Hamburg, Germany). The 50 nm-thick carbon foils, each with an area density of 10 µg cm^{-2} and purity of 99.997% on temporary glass supports, were purchased from GoodFellow Ltd. (Huntingdon, UK). Carbon coated TEM copper grids (3.05 mm diameter and 200 mesh) were obtained from Plano Ltd. (Bolton, UK), Ethanol (C_2H_5OH) with a purity of 99%, which was needed for cleaning supporting materials during the deposition procedure, was purchased from SAV LP Ltd. (Flintsbach am Inn, Germany), and ultrapure water (H_2O), required for the detachment of the carbon foil from the supporting glass, was obtained by means of a Millipore water purification system. Aluminum sample holders 20 mm in diameter with a 5 mm-diameter aperture in the center were manufactured at the Physikalisch-Technische Bundesanstalt (Braunschweig, Germany). The thickness of these sample holders was 1 mm.

Mounting of the Carbon Substrate: Aluminum sample holders and all glassware were thoroughly cleaned with ethanol in an ultrasonic bath. A slice of the carbon foil on temporary glass supports was cut with a scalpel to the size of the aluminum sample holder. Afterward, the glass containing the carbon foil slice was slowly immersed in ultrapure water at a small inclination angle until the water surface reached the lower edge of the carbon film. As the film started to detach from the glass, the glass was immersed deeper until the carbon foil completely detached and floated free on the water surface. The sample holder was then submerged in water beneath the floating slice of carbon foil at an angle of about 45° relative to the normal of the water surface. The floating slice of carbon foil was then collected on the flat face of the sample holder and dried for 24 h in ambient air at room temperature prior to use. Following the same procedure, TEM grids were also covered with carbon foils.

Deposition: Deposition of AuNPs on carbon foils attached to the sample holder was carried out using three different techniques. First, the drop-casting technique was applied. This involved stirring the AuNP solution to obtain homogeneity, where an Eppendorf pipette (Hamburg, Germany) was used to cast a 0.5 µL droplet of this AuNP solution onto

the sample holder, which was covered with 50 nm-thick carbon foil. The droplet was left for 24 h to dry in ambient air at room temperature. Five different samples were prepared at different time intervals and then examined over a period of 1 year.

The second of these techniques was the spin-coating procedure, which was applied using a spin-coater SM-150 from Sawatec AG (Sax, Swiss). To allow placement of the sample holder covered with 50 nm-thick carbon foil onto the spin-coater, the holder was attached to a wafer using adhesive tape. After stirring the AuNP solution, an Eppendorf pipette was used to cast a 0.5 µL droplet of AuNP solution onto the carbon foil above the sample holder and then spun with a rotation speed of 1000 rpm for 60 s.

The third technique involved the deposition of microdrops generated by an autodrop pipette of a microdrop purchased from microdrop Technologies Ltd. (Norderstedt, Germany). The pipette's piezo driver voltage and the pulse interval between two subsequent drops were calibrated using water as the test liquid. After stirring the AuNP solution, between one and one hundred microdroplets (with a diameter and volume of about 80 µm and 300 pL, respectively) were placed at a selected position on the sample holder using a piezo driver voltage $U = 57$ V and a pulse length $\Delta t = 27$ µs.

AuNP Characterization: AuNP samples produced using the three techniques described above were characterized with respect to size, shape, distribution, and area density using images produced with a Supra 35VP Gemini scanning electron microscope from Carl Zeiss AG (Jena, Germany) equipped with a STEM detector. The SEM was operated at an acceleration voltage of 30 kV. The AuNPs samples that were prepared at different times over the course of a year were repeatedly analyzed with respect to size distribution, area density, and degree of clustering using SEM and STEM during a 1 year period.

Analysis of AuNP Size Distribution: The size distribution of AuNPs was determined from STEM images of regions with sub-monolayers, where the diameter of 100 isolated AuNPs was measured using the line tool function of the software ImageJ (Washington, DC, USA).[46,47]

Figure 8 shows the cumulative frequency of AuNPs as function of their size for three different measurement times, where the measured diameters of the AuNPs can be seen to range from 9.0 to 13.5 nm. The highest frequency was observed for AuNPs with diameters between 10.5 and 11.5 nm, with a mean diameter of 11.1 ± 1.8 nm. The STEM measurements of five different samples carried out over a 1 year period show that the distributions of AuNP remain relatively constant with time.

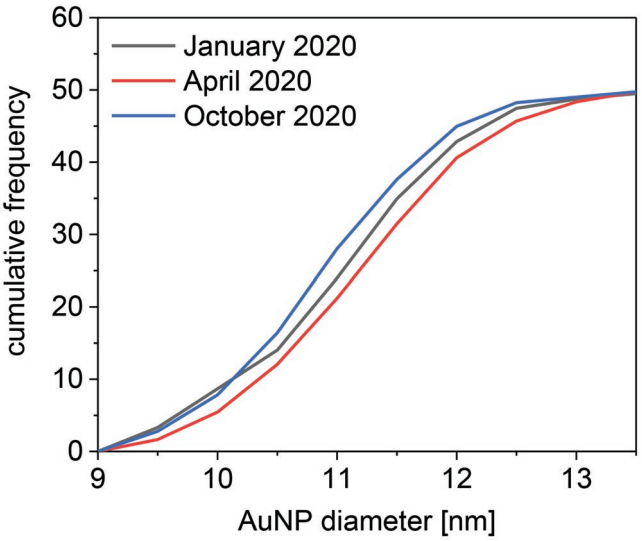

Figure 8. Diameter distribution of AuNPs measured over a 1 year period, where the three curves represent the distribution of diameters measured at different times.

Analysis of AuNP Area Density: To measure the area density, STEM images were converted into black and white images by adjusting the background threshold and then determining the area covered by AuNPs using the "Analyze Particles" function of the software ImageJ.[46,47] Preliminary quantification of the variation in area density across the sample can be found in the supporting information, where the results are listed in Table S1, Supporting Information, and depicted in Figure S3, Supporting Information.

Supporting Information

Supporting Information is available from the Wiley Online Library or from the author.

Acknowledgements

This work was funded by the Deutsche Forschungsgemeinschaft (DFG, German Research Foundation) under grant number 386872118. The authors thank Elisabetta Gargioni and Florian Schulz for providing the gold nanoparticles and Andreas Pausewang for the construction of the sample holders. The assistance and support of Philipp Ranitzsch (with the microdrop technique), Maikel Petrich (for use of the spin-coater), Detlef Bergmann (with SEM and STEM measurements), and Peter Hinze and Alexander Ruhz (with SEM measurements) are also gratefully acknowledged. The authors acknowledge DESY (Hamburg, Germany), a member of the Helmholtz Association HGF, for the provision of experimental facilities. Parts of this research were carried out at PETRA III and the authors thank Christoph Schlueter, Andrei Hloskovsky, and Patrick Lömker for their assistance in using beamline P22 with the HAXPES setup. Beamtime was allocated for proposal I-20200068.

Open access funding enabled and organized by Projekt DEAL.

Conflict of Interest

The authors declare no conflict of interest.

Data Availability Statement

The data that support the findings of this study are available from the corresponding author upon reasonable request.

Keywords

deposition, drop-casting, gold nanoparticles, spin-coating

Received: July 19, 2022
Revised: August 17, 2022
Published online: September 12, 2022

[1] G. Frens, *Nat. Phys. Sci.* **1973**, *241*, 20.
[2] B. V. Enustun, J. Turkevich, *J. Am. Chem. Soc.* **1963**, *85*, 3317.
[3] D. A. Giljohann, D. S. Seferos, W. L. Daniel, M. D. Massich, P. C. Patel, C. A. Mirkin, *Angew. Chem., Int. Ed.* **2010**, *49*, 3280.
[4] M. Fan, Y. Han, S. Gao, H. Yan, L. Cao, Z. Li, X.-J. Liang, J. Zhang, *Theranostics* **2020**, *10*, 4944.
[5] S. Vial, R. L. Reis, J. M. Oliveira, *Curr. Opin. Solid State Mater. Sci.* **2017**, *21*, 92.

[6] C. Carnovale, G. Bryant, R. Shukla, V. Bansal, *ACS Omega* **2019**, *4*, 242.
[7] J. Zhang, L. Mou, X. Jiang, *Chem. Sci.* **2020**, *11*, 923.
[8] J. Schuemann, R. Berbeco, D. B. Chithrani, S. H. Cho, R. Kumar, S. J. McMahon, S. Sridhar, S. Krishnan, *Int. J. Radiat. Oncol., Biol., Phys.* **2016**, *94*, 189.
[9] J. Schuemann, A. Bagley, R. Berbeco, K. Bromma, K. T. Butterworth, H. Byrne, D. B. Chithrani, S. H. Cho, J. R. Cook, V. Favaudon, Y. H. Gholami, E. Gargioni, J. F. Hainfeld, F. Hespeels, A.-C. Heuskin, U. M. Ibeh, Z. Kuncic, S. Kunjachan, S. Lacombe, S. Lucas, F. Lux, S. J. McMahon, D. Nevozhay, W. Ngwa, J. D. Payne, S. Penninckx, E. Porcel, K. M. Prise, H. Rabus, S. M. Ridwan, et al., *Phys. Med. Biol.* **2020**, *65*, 21RM02.
[10] J. F. Hainfeld, D. N. Slatkin, H. M. Smilowitz, *Phys. Med. Biol.* **2004**, *49*, N309.
[11] Z. Kuncic, S. Lacombe, *Phys. Med. Biol.* **2018**, *63*, 02TR01.
[12] D. Sakata, I. Kyriakou, H. N. Tran, M.-C. Bordage, A. Rosenfeld, V. Ivanchenko, S. Incerti, D. Emfietzoglou, S. Guatelli, *Phys. Med.* **2019**, *63*, 98.
[13] P. Zygmanski, E. Sajo, *Br. J. Radiol.* **2016**, *89*, 20150200.
[14] W. B. Li, A. Belchior, M. Beuve, Y. Z. Chen, S. D. Maria, W. Friedland, B. Gervais, B. Heide, N. Hocine, A. Ipatov, A. P. Klapproth, C. Y. Li, J. L. Li, G. Multhoff, F. Poignant, R. Qiu, H. Rabus, B. Rudek, J. Schuemann, S. Stangl, E. Testa, C. Villagrasa, W. Z. Xie, Y. B. Zhang, *Phys. Med.* **2020**, *69*, 147.
[15] W. B. Li, M. Beuve, S. D. Maria, W. Friedland, B. Heide, A. P. Klapproth, C. Y. Li, F. Poignant, H. Rabus, B. Rudek, J. Schuemann, C. Villagrasa, *Phys. Med.* **2020**, *80*, 383.
[16] H. Rabus, W. B. Li, C. Villagrasa, J. Schuemann, P. A. Hepperle, L. de la Fuente Rosales, M. Beuve, S. D. Maria, A. P. Klapproth, C. Y. Li, F. Poignant, B. Rudek, H. Nettelbeck, *Phys. Med.* **2021**, *84*, 241.
[17] F. Moradi, K. R. Saraee, S. F. Sani, D. A. Bradley, *Radiat. Phys. Chem.* **2021**, *180*, 109294.
[18] E. Vlastou, S. Diamantopoulos, E. P. Efstathopoulos, *Phys. Med.* **2020**, *80*, 57.
[19] R. Casta, J.-P. Champeaux, P. Moretto-Capelle, M. Sence, P. Cafarelli, *J. Nanopart. Res.* **2015**, *17*, 3.
[20] G. Yang, D. T. Hallinan, *Sci. Rep.* **2016**, *6*, 35339.
[21] M. Sharma, A. T. Tan, B. D. Smith, A. J. Hart, J. C. Grossman, *ACS Appl. Nano Mater.* **2019**, *2*, 1146.
[22] H. Song, Y. M. Lim, H. W. Kwon, M. S. Lee, Y. T. Yu, *J. Ceram. Process. Res.* **2007**, *8*, 341.
[23] A. Yanguas-Gil, *Growth and Transport in Nanostructured Materials*, Springer International Publishing, New York **2017**.
[24] M. L. Reed, G. K. Fedder, in *Handbook of Sensors and Actuators* (Ed: T. Fukuda), Elsevier, Amsterdam Am New York **1998**, Ch. 2.
[25] A. V. Rane, K. Kanny, V. K. Abitha, S. Thomas, in *Synthesis of Inorganic Nanomaterials: Advances and Key Technologies* (Ed: S. Bhagyaraj), Elsevier Ltd. Woodhead Publishing, Cambridge **2018**, Ch. 5.
[26] D. Zhang, J. Hu, K. M. Kennedy, I. P. Herman, *Langmuir* **2016**, *32*, 8467.
[27] M. M. Velázquez, T. Alejo, D. López-Díaz, B. Martín-García, M. D. Merchán, in *Two-Dimensional Materials – Synthesis, Characterization and Potential Applications*, InTechOpen, London **2016**, Ch. 2.
[28] S. A. Hussain, B. Dey, D. Bhattacharjee, N. Mehta, *Heliyon* **2018**, *4*, e01038.
[29] T. Ishida, Y. Tachikiri, T. Sako, Y. Takahashi, S. Yamada, *Appl. Surf. Sci.* **2017**, *404*, 350.
[30] J. Puetz, M. A. Aegerter, in *Sol–Gel Technologies for Glass Producers and Users* (Eds: M. A. Aegerter, M. Mennig), Springer US, Boston, MA **2004**, Ch. 2.2.1.
[31] S. Hosseingholilou, D. Dorranian, M. Ghoranneviss, *Gold Bull.* **2020**, *53*, 1.
[32] A. de Leon, R. C. Advincula, in *Intelligent coatings for corrosion control* (Eds: A. Tiwari, L. Hihara, J. Rawlins), Butterworth-Heinemann, Amsterdam **2015**, Ch. 11.
[33] T. P. Bigioni, X.-M. Lin, T. T. Nguyen, E. I. Corwin, T. A. Witten, H. M. Jaeger, *Nat. Mater.* **2006**, *5*, 265.
[34] S. Macis, G. Cibin, V. Maggi, G. Baccolo, D. Hampai, B. Delmonte, A. D'Elia, A. Marcelli, *Condens. Matter* **2018**, *3*, 21.
[35] Y. Zhao, J. S. Marshall, *Phys. Fluids* **2008**, *20*, 043302.
[36] Y.-K. Hong, H. Kim, G. Lee, W. Kim, J.-I. Park, J. Cheon, J.-Y. Koo, *Appl. Phys. Lett.* **2002**, *80*, 844.
[37] M. Israelowitz, J. Amey, T. Cong, R. Sureshkumar, *J. Nanomater.* **2014**, *2014*, 639458.
[38] L. A. DeSilva, M. Thakurdesai, T. M. Bandara, J. Preston, W. Johnson, A. Gaquere-Parker, S. Survase, *Appl. Phys. A* **2018**, *124*, 314.
[39] D. P. Birnie, in *Sol-Gel Technologies for Glass Producers and Users* (Eds: M. A. Aegerter, M. Mennig), Springer US, Boston, MA **2004**, Ch. 2.2.2.
[40] M. P. Romano, M. G. Lionetto, A. Mangone, A. R. De Bartolomeo, M. E. Giordano, D. Contini, M. R. Guascito, *Anal. Chim. Acta* **2022**, *1206*, 339556.
[41] P. J. Yunker, T. Still, M. A. Lohr, A. G. Yodh, *Nature* **2011**, *476*, 308.
[42] D. Mampallil, H. B. Eral, *Adv. Colloid Interface Sci.* **2018**, *252*, 38.
[43] H. Vandeparre, M. Piñeirua, F. Brau, B. Roman, J. Bico, C. Gay, W. Bao, C. N. Lau, P. M. Reis, P. Damman, *Phys. Rev. Lett.* **2011**, *106*, 224301.
[44] B. Pacakova, J. Vejpravova, A. Repko, A. Mantlikova, M. Kalbac, *Carbon* **2015**, *95*, 573.
[45] C. Kunstmann-Olsen, D. Belić, D. Bradley, M. Grzelczak, *Chem. Mater.* **2016**, *28*, 2970.
[46] ImageJ, https://imagej.nih.gov/ij/download.html (accessed: January 2020).
[47] C. Schneider, W. Rasband, K. Eliceiri, *Nat. Methods* **2012**, *9*, 671.

